Hypermeander of Spirals; Local Bifurcations and Statistical Properties

Peter Ashwin
School of Mathematical Sciences,
Laver Building,
University of Exeter,
Exeter EX4 4QE, UK

Ian Melbourne
Department of Mathematics
University of Houston
Houston, TX 77204-3476, USA

Matthew Nicol
Department of Mathematics and Statistics
University of Surrey
Guildford GU2 7XH, UK

January 23, 2001

Abstract

In both experimental studies and numerical simulations of waves in excitable media, rigidly rotating spiral waves are observed to undergo transitions to complicated spatial dynamics with long-term Brownian-like motion of the spiral tip. This phenomenon is known as hypermeander.

In this paper, we review a number of recent results on dynamics with non-compact group symmetries and make the case that hypermeander may occur at a codimension two bifurcation from a rigidly rotating spiral wave. Our predictions are based on center bundle reduction (Sandstede, Scheel & Wulff), and on central limit theorems and invariance principles for group extensions of hyperbolic dynamical systems. These predictions are confirmed by numerical simulations of the center bundle equations.

1 Introduction

Spiral waves occur in chemical reactions, such as the Belousov-Zhabotinskii (BZ) reaction, and in numerical simulations of partial differential equations (PDEs) modeling excitable media. There is a variety of transitions from rigidly rotating spiral waves to more complicated states including spirals that *quasiperiodically meander* and *linearly drift* [44, 26], *retracting waves* [28], and *hypermeander* [35]. Surveys of spiral wave behavior in chemical reactions and in PDE models can be found in [22, 23, 42].

The transitions to meander and linear drift are now well-understood [4, 14, 39, 19] and are a consequence of the Euclidean symmetry in the problem. The key technical tool here is the center bundle reduction method of Sandstede *et al.* [39]. A partial explanation of the transition to retracting waves can be found in [2].

The transition to hypermeander was first documented by Rossler & Kahlert [35], see also Winfree [42]. Here the dynamics is "complicated/chaotic" and the motion of the spiral is reminiscent of a random walk, or even Brownian motion.

Biktashev & Holden [6] suggested that chaotic dynamics at the orbit space level could lead to square root growth rates for the translation drift hence providing a mechanism for hypermeander. Nicol *et al.* [29, 3]) proved this to be the case under certain hyperbolicity assumptions on the orbit space dynamics, and showed furthermore that the drift converges in distribution to a standard n-dimensional normal distribution. More recently, Field *et al.* [16] have obtained results on approximation by Brownian motion (weak and almost sure invariance principles).

As in the case of meander [19], it is only within the context of local bifurcation theory that the global dynamics described in [6, 16, 29] can manifest itself as hypermeander in physical space. Hence, the global results must be combined with the local bifurcation theory approach in [14, 19].

Fiedler & Turaev [15] considered Takens-Bogdanov bifurcation from a rotating wave in systems with Euclidean symmetry and, using the approach in [14], made the remarkable observation that the homoclinic orbit in the orbit space (which is of course nonchaotic) leads to Brownian motion-like behavior in physical space. However, this behavior is not hypermeander (indeed, no such claim was made in [15]) as it is associated with an asymptotic slowing down of the large-scale tip motion. It is natural to consider the remaining codimension two bifurcations (steady-state/Hopf or Hopf/Hopf mode-interactions) since these are known to produce chaotic dynamics [20].

In this paper, we focus on Hopf/Hopf bifurcation from rotating waves in systems with Euclidean symmetry (our investigations indicate that the steady-state/Hopf mode-interaction leads to very similar conclusions) and attempt to explain the onset of hypermeander in terms of the chaotic dynamics arising in this local bifurcation. The explanation relies on the following theoretical ingredients:

1. Codimension two Hopf/Hopf bifurcation from rigidly rotating spiral waves in the underlying chemical reaction or modeling PDE leads via center bundle reduction [39] to a 7-dimensional skew-product ODE.

2. A consequence of the chaotic dynamics associated with Hopf/Hopf (or steady-state/Hopf) bifurcation is that the evolution of the translation coordinate for the skew product ODE, and hence the motion of the spiral tip in the underlying PDE, is asymptotic to a Brownian motion [29, 16].

The new feature of this paper is the proposed explanation of hypermeander as arising through the combination of these techniques from local and global dynamical systems theory. Furthermore, we present numerical results from truncations of the center bundle equations that indeed yield Brownian motion-like trajectories for the spiral tip, in accordance with our theoretical predictions.

The remainder of this paper is organized as follows. In Section 2, we recall certain aspects relating to hypermeander in experimental and numerical studies of spiral waves in excitable media. In Section 3, we review and analyze transitions of spiral waves from the perspective of local bifurcation theory, concentrating on the cases of Hopf bifurcation, Takens-Bogdanov bifurcation and the Hopf/Hopf bifurcation mentioned above. In Section 4, we survey recent results that make rigorous the connection between the low-dimensional chaos that occurs in the steady-state/Hopf and Hopf/Hopf mode-interactions and the Brownian-like motion of hypermeander.

Finally, in Section 5, we present an overview of our proposed explanation of hypermeander of spiral waves, with a discussion of how close this is to being a completely rigorous explanation.

2 Experimental and numerical results

In the simplest instance, planar spiral waves rigidly rotate and the tip of the spiral traces out a circle in the plane. Such a solution is called a *rotating wave* and its time evolution corresponds to rigid rotation.

As system parameters are varied, there is a variety of transitions to spiral waves that exhibit more complicated motions as they rotate. Zykov [44] and Winfree [42] illustrate this with a two parameter bifurcation diagram for the FitzHugh-Nagumo equation, see Figure 1. These transitions are well-confirmed both in experimental systems [22, 25, 33, 41] and in numerical simulations of two-dimensional excitable media such as the FitzHugh-Nagumo equation or the Oregonator [22, 26]. Rigidly rotating spirals are observed in the region of parameter space between the transition curves ∂R and ∂M in Figure 1.

Meander and linear drift The simplest transition from rigidly rotating spirals is to *meandering* spirals where the tip of the spiral traces out a flower-like pattern (Figure 2(b)). These are quasiperiodic two-frequency solutions, and the spiral tip undergoes an epicycle motion superimposed on the basic spiral wave circle. Barkley *et al.* [5] explained this transition as a Hopf bifurcation from a rotating wave, as confirmed experimentally in [41]. The Hopf bifurcation takes place along the curve ∂M in Figure 1.

There is a codimension two point where the frequency ω_{Hopf} of the Hopf bifurcation is close to the frequency ω_{rot} of the rotating wave, leading to a remarkable resonance phenomenon where the amplitude of the epicycle is large even close to the Hopf bifurcation. The 'petals' of the flower are now well-defined and may point inwards or outwards (Figure 2(c,d)) depending on whether the epicycle has the same orientation to the motion on the circle or the reverse orientation; this orientation has been referred to as the 'petality' of the path. We note that the circle representing the rigidly rotating spiral corresponds to the flower away from resonance and to the petals near resonance.

At $\omega_{\text{Hopf}} = \omega_{\text{rot}}$, the petality changes from inwards to outwards, the radius of the flower grows infinitely large, and the spiral appears to drift linearly off to infinity (Figure 2(e)).

Barkley [4] gave the first explanation of the resonant meandering and linear drift, and highlighted the need to discuss the full Euclidean $\mathbf{E}(2)$ symmetry in models including translations as well as rotations. Li *et al.* [25] obtained experimental confirmation of this explanation. The first rigorous results were due to Wulff [43] and culminated in the work of Sandstede *et al.* [39]. (See also [14, 18, 38].) As a result, meander and linear drift are now understood in terms of a codimension two bifurcation from a rotating wave in a system with $\mathbf{E}(2)$ symmetry. Section 3(a) reviews this work in more detail below.

Interpretations in physical space When speaking of the motion of the tip of a spiral wave, there is the implicit assumption that the spiral tip (or even the complete spiral structure) is well-defined throughout the chaotic motion. That is, the *shape* of the spiral undergoes negligible change relative to the change in position, or *drift* of the spiral in the plane.

By contrast, one can construct models with periodic solutions that are spiral-like for part of the period, but not resembling a spiral for another part of the period. In such a situation, it is clearly not possible to discuss motion of the spiral tip.

There is no problem of interpretation for a rigidly rotating spiral, since the shape of the spiral is constant by assumption. Recall that the transition from rotating spirals to meandering spirals is a Hopf bifurcation. Hence, in addition to the quasiperiodic meander of the spiral, there is a $2\pi/\omega_{\text{Hopf}}$-periodic modulation of the shape of the

spiral given by the modes excited in the Hopf bifurcation. It is readily verified (see for example Golubitsky *et al* [19]) that the magnitude of the change in shape is identical to the magnitude of the change in drift: both scale as $\sqrt{\lambda}$ where λ is the bifurcation parameter. Nevertheless, as described in more detail in [19], the shape change is a disorganized localized motion whereas the drift is a rigid global planar motion. As a result, it makes sense to view the motion of the spiral as a rigid quasiperiodic epicyclic motion in the plane combined with a periodic fluctuation of the shape of the spiral.

Hypermeander Hopf bifurcation from rigidly rotating spirals leads to meandering spirals which are two-frequency quasiperiodic states. Rossler & Kahlert [35] discovered a further transition to a more complicated state known as *hypermeandering* spirals. The motion in the plane is similar to meandering, except that there is an additional Brownian motion-like component, so that the center of the flower pattern undergoes a random walk over long timescales.

At present, this transition to hypermeander remains somewhat controversial [6]. Experimentally, the transition appears to take place along the curve ∂C in Figure 1. However, in several instances, careful simulations have revealed apparent hypermeander to be a (long) transient, before the motion settles down to an ordinary meander; see Figure 3.

It is worth mentioning that, as was the case for meander, the fluctuation in the shape of a hypermeandering spiral is again negligible so that it makes sense to track the motion of the spiral in the plane. This is strongly indicative [19] that hypermeander is the result of a local bifurcation and can be modelled using low dimensional dynamics.

3 Local bifurcations from rigidly rotating spirals

Let $u(x,t)$ be a solution to a PDE (such as the FitzHugh-Nagumo equations or the Oregonator) modeling a homogeneous excitable medium. Here $x \in \mathbb{R}^2$ denotes the spatial variables and t is time. The vector u represents the concentrations of the active chemicals in the reaction.

As a result of the homogeneity of the excitable media, the modeling PDE is equivariant with respect to rotations, reflections and translations in the plane, and so has Euclidean $\mathbf{E}(2)$ symmetry. This means that if $u(x,t)$ is a solution, then so is $u(\gamma x, t)$ for each $\gamma \in \mathbf{E}(2)$.

The solution $u(x,t)$ is a *relative equilibrium* if $u(x,t) = u_0(\gamma(t)x)$ where $\gamma(t) \in \mathbf{E}(2)$. Thus, time evolution corresponds to rigid spatial motion. By continuity, $\gamma(t)$ actually lies in the special Euclidean group $\mathbf{SE}(2)$ consisting of rotations and translations. Writing the PDE as an evolution equation $u_t = F(u)$ on some Banach space,

an equivalent formulation is that $(dF)_{u_0} = \xi u_0$ for some $\xi \in L\mathbf{SE}(2)$, where $L\mathbf{SE}(2)$ is the Lie algebra of $\mathbf{SE}(2)$. In this case, $\gamma(t) = \exp(t\xi)$.

Suppose that $u_0(x)$ is a (one-armed) spiral solution. Note that $u_0(x)$ itself has no symmetry. Generically (and in particular for most small perturbations) the solution will drift along the $\mathbf{SE}(2)$-group orbit. Moreover, this drift is generically a rotation [1]. Hence, $u(x,t) = u_0(R_{\omega_{\rm rot}t}x)$ is a rigidly rotating spiral wave. (The existence of such solutions has been proved rigorously by Scheel [40].) Again, we can write $(dF)_{u_0} = \xi u_0$ where $\xi \in L\mathbf{SO}(2)$. Let $L = (dF)_{u_0} - \xi u_0$. Since $\dim \mathbf{SE}(2) = 3$, it follows that L has three eigenvalues on the imaginary axis forced by symmetry. If the remainder of the spectrum is bounded away from the imaginary axis into the left-half-plane, then the rotating wave $u(x,t)$ is asymptotically stable. If there is any spectrum with positive real part, then $u(x,t)$ is unstable.

A local bifurcation occurs when eigenvalues cross the imaginary axis. We suppose that at the bifurcation point, there are finitely many eigenvalues on the imaginary axis, and the remainder of the spectrum is bounded into the left-half-plane. Then Sandstede *et al.* [39] proved, under certain additional technical hypotheses, that there is a reduction to a finite-dimensional ODE on the *center bundle* $X \times \mathbf{SE}(2)$. The dimension of the center bundle is equal to the number of eigenvalues on the imaginary axis.

We identify $\mathbf{SE}(2)$ with $S^1 \times \mathbb{C}$ and use coordinates $(x, \varphi, v) \in X \times S^1 \times \mathbb{C}$. Also, we suppress bifurcation parameters for the moment. A computation using $\mathbf{SE}(2)$-equivariance shows that the center bundle equations have the skew product form [14, 18]

$$\dot{x} = f_x(x), \quad \dot{\varphi} = f_\varphi(x), \quad \dot{v} = e^{i\varphi} f_v(x), \tag{3.1}$$

where $f_x : X \to X$, $f_\varphi : X \to \mathbb{R}$, $f_v : X \to \mathbb{R}^2$. The 'origin' $x = 0$ corresponds to the underlying spiral solution, so we can assume that

$$f_x(0) = 0, \quad f_\varphi(0) = \omega_{\rm rot}, \quad f_v(0) = 0.$$

The skew product equations (3.1) can be thought of as an $\mathbf{SE}(2)$ group extension of the base dynamics $\dot{x} = f_x(x)$ on X, see [29]. In the original PDE model [19] the base dynamics on X represents the 'shape variables' which modulate the shape of the underlying 'trivial solution' (in the case, the rigidly rotating spiral wave) while the group variables (φ, v) in $\mathbf{SE}(2)$ describe the rotation and translation drift of the solution in the plane. Here, v can be thought of as modelling the location and φ the orientation of a fixed reference point on the spiral wave; for example the spiral tip.

We discuss in detail three bifurcations from rigidly rotating spiral waves; (a) and (b) reviews previous work, including some new simulations for (b), whereas (c) is one of the simplest local bifurcations that has all the ingredients necessary to generate hypermeandering solutions.

(a) Hopf bifurcation: $X = \mathbb{R}^2 \cong \mathbb{C}$, $(df_x)_0 = i\omega_{\text{Hopf}}$,

(b) Takens-Bogdanov bifurcation: $X = \mathbb{R}^2$, $(df_x)_0 = \begin{pmatrix} 0 & 1 \\ 0 & 0 \end{pmatrix}$, and

(c) Hopf/Hopf bifurcation: $X = \mathbb{R}^4 \cong \mathbb{C}^2$, $(df_x)_0 = \begin{pmatrix} i\omega_1 & 0 \\ 0 & i\omega_2 \end{pmatrix}$.

We could equally well study steady-state/Hopf bifurcation with $X = \mathbb{R}^3 \cong \mathbb{C} \times \mathbb{R}$ and $(df_x)_0 = \begin{pmatrix} i\omega & 0 \\ 0 & 0 \end{pmatrix}$. Both steady-state/Hopf and Hopf/Hopf bifurcation have the ingredients necessary to generate hypermeander. Since our numerical simulations of the two cases lead to similar behaviour, we focus for the sake of brevity on the Hopf/Hopf case.

(a) Hopf bifurcation: meander and linear drift

In the case of Hopf bifurcation, a pair of complex eigenvalues cross the imaginary axis at $\pm i\omega_{\text{Hopf}}$ and there is a five-dimensional center bundle $\mathbb{C} \times \mathbf{SE}(2)$. We briefly review the calculation of the solutions to the center bundle equations (3.1). For more details, see [14, 18, 19].

Let $\lambda \in \mathbb{R}$ denote the bifurcation parameter. Hopf bifurcation leads to a branch of $2\pi/\omega_{\text{Hopf}}(\lambda)$-periodic solutions in the $\dot{x}$-equation, where $\omega_{\text{Hopf}}(0) = \omega_{\text{Hopf}}$. Substituting into the $\dot{\varphi}$-equation in (3.1) and integrating yields

$$\varphi(t) = \omega_{\text{rot}}(\lambda)t + \widetilde{\varphi}(t),$$

where $\omega_{\text{rot}}(0) = \omega_{\text{rot}}$ and $\widetilde{\varphi}(t)$ is $2\pi/\omega_{\text{Hopf}}(\lambda)$-periodic. The $\dot{v}$-equation can now be written in the form

$$\dot{v} = e^{i\omega_{\text{rot}}(\lambda)t} H(t),$$

where $H(t)$ is a $2\pi/\omega_{\text{Hopf}}(\lambda)$-periodic function. Expanding H as a Fourier series, it follows that $\dot{v}$ has frequencies $\omega_{\text{rot}}(\lambda) + n\omega_{\text{Hopf}}(\lambda)$ for $n = 0, 1, 2, \cdots$. Resonance occurs when

$$\omega_{\text{rot}}(\lambda) + n\omega_{\text{Hopf}}(\lambda) = 0$$

for some n. In the absence of resonance, $v(t)$ is a two-frequency quasiperiodic function. The graph of $(\varphi(t), v(t))$ describes the motion of the spiral tip in the plane and is a epicyclic flower pattern as shown in Figure 2(b). (Figure 2(b) is taken from [19] and incorporates also the shape change of the spiral.)

At resonance, there is an additional linear term in $v(t)$ (due to the constant term in $\dot{v}$) resulting in Figure 2(e). The motion of the tip close to resonance is shown in Figure 2(c,d).

(b) Takens-Bogdanov bifurcation

The consequences of a Takens-Bogdanov bifurcation were discussed in [15]. One obtains a two-dimensional center manifold $X = \mathbb{R}^2$ and hence a five-dimensional center bundle $\mathbb{R}^2 \times \mathbf{SE}(2)$ for the skew product equations (3.1). A universal unfolding of the singularity on $\mathbb{R}^2$ is given by

$$f_x(x, y) = (y, \lambda + \mu y + x^2 \pm xy),$$

where $(x, y) \in \mathbb{R}^2$ and $\lambda, \mu \in \mathbb{R}$ are the unfolding parameters. The main effect of the $\pm$ is on the stability of certain limit cycles that arise in the dynamics of the unfolding; the minus sign ensures that these limit cycles are asymptotically stable.

There is a curve $C \subset \mathbb{R}^2$ defined in a neighborhood of the origin such that the (x, y)-equations have a homoclinic loop for $(\lambda, \mu) \in C$. Fiedler & Turaev [15] proved the existence of Brownian-motion like dynamics in the skew product (3.1) for such parameter values. Note that the dynamics in the noncompact group extension $\mathbb{R}^2 \times \mathbf{SE}(2)$ exhibits random behavior even though the base dynamics on $\mathbb{R}^2$ is nonchaotic.

In practice, it is not possible to choose parameters (λ, μ) lying exactly on C, but we can consider parameters that are close. For an open set of parameters there is an asymptotically stable limit cycle on the center manifold X corresponding to flow-invariant tori in the skew product

$$\begin{aligned}
\dot{x} &= y \\
\dot{y} &= \lambda + \mu y + x^2 - xy \\
\dot{\varphi} &= f_\varphi(x, y) \\
\dot{v} &= e^{i\varphi} f_v(x, y)
\end{aligned}$$

and hence to meandering spiral waves in the application. For parameters close enough to C, there is a transient dynamics that behaves as predicted in [15].

In Figure 4, we show the skew product dynamics for the parameter values $\lambda = -0.001$, $\mu = -0.0226177$ which lie close to C. (We take $f_\varphi = \omega_{\text{rot}} + ax + by$, $f_v = \alpha x + \beta y$, where $a = 1.2$, $b = 0.7$, $\alpha = 0.8 + 0.5i$, $\beta = 0.6 + 0.7i$, but these choices are not so important.) The dynamics with and without the transient are shown in Figure 4(a) and (b) respectively.

Figure 4(a) is reminiscent of certain numerical simulations of hypermeander in reaction-diffusion equations, see Figure 3. It is worth stressing that Figure 4(a) is obtained by numerically integrating the five-dimensional center bundle equations whereas Figure 3 is obtained by integrating an approximation of the infinite-dimensional FitzHugh-Nagumo equations.

Note however that the parameters λ and μ have to be chosen extremely close to the curve C on which the homoclinic loop exists. Moreover, the transient is quite

short and the initial conditions $(x_0, y_0) \in \mathbb{R}^2$ have to be chosen sufficiently distant from the limit cycle.

(c) Hopf/Hopf mode-interaction

For Hopf/Hopf bifurcation, there is a four-dimensional center manifold $X = \mathbb{C}^2 = \mathbb{R}^4$ and the linearization $(df_x)_0$ typically has ω_1/ω_2 irrational. To unfold the linear part of such a bifurcation one needs two parameters in addition to the angular frequencies ω_i, $i = 1, 2$. A system near such a bifurcation point can be transformed using near-identity transformations into a polynomial normal form [20] through arbitrarily high order. This process introduces normal form phase-shift symmetry which aids in the analysis of the dynamics but suppresses the dynamics that we are interested in. In particular, the chaotic dynamics that occurs in the Hopf/Hopf mode-interaction arises from terms in the tail that break the normal form symmetry. Hence we consider a system of equations (using real variables only) that does not have normal form symmetry:

$$\begin{aligned}
\dot{w} &= \lambda_1 w + \omega_1 x - (0.1 + y^2)w^3 \\
\dot{x} &= -\omega_1 w + \lambda_1 x - w^2 x \\
\dot{y} &= \lambda_2 y + \omega_2 z - (0.1 + w^2)y^3 \\
\dot{z} &= -\omega_2 y + \lambda_2 z - y^2 z \\
\dot{\varphi} &= f_\varphi(w, x, y, z) \\
\dot{v} &= e^{i\varphi} f_v(w, x, y, z)
\end{aligned} \tag{3.2}$$

where $(w, x, y, z) \in \mathbb{R}^4$ and $(\varphi, v) \in \mathbf{SE}(2)$. There are four parameters; the Hopf frequencies ω_1, ω_2 and the bifurcation parameters λ_1, λ_2.

For simplicity, we take f_v to be real and we suppose that f_φ and f_v depend only on w. In particular, we take

$$\begin{aligned}
f_\varphi(w, x, y, z) &= a_1 + a_2 w + a_3 w^2 + a_4 w^3 \\
f_v(w, x, y, z) &= b_1 + b_2 w + b_3 w^2 + b_4 w^3
\end{aligned}$$

where a_j, $b_j \in \mathbb{R}$. As we will see, this form of f_φ, f_v is sufficient to give the expected generic behaviour. Addition of explicit dependence on x, y, z or choosing f_v complex does not change the qualitative drifting behaviour as long as both of the Hopf modes are excited. We use the parameter values

$$(a_1, a_2, a_3, a_4) = (0.1, 0.2, 0.3, 0.4), \quad (b_1, b_2, b_3, b_4) = (0.1, 0.2, 0.5, -0.2),$$

which are chosen to avoid having any obvious symmetries. Qualitatively similar results were found for other parameter values, although no systematic study of the parameter space was attempted.

It is well-known [20] that Hopf/Hopf mode-interaction leads to invariant tori in the (w, x, y, z)-equations. Generically, the dynamics on an invariant torus is phase-locked to a periodic solution, but with high probability the flow is a two-frequency quasiperiodic motion. On further variation of parameters, the invariant tori break up leading to chaotic dynamics [27, 20]. We consider these two cases in turn.

Quasiperiodic dynamics The choice of parameters $(\lambda_1, \lambda_2, \omega_1, \omega_2) = (1, 1, 3.8, 1.5)$ leads to large-scale quasiperiodic dynamics, see Figure 5(a). Typically, the dynamics in the Euclidean extension is bounded [24, 29] so that there is a three-frequency quasiperiodic motion (the additional frequency coming from the underlying rotating wave). Figure 5(b) confirms this theoretical prediction.

Chaotic dynamics The choice of parameters $(\lambda_1, \lambda_2, \omega_1, \omega_2) = (3, 2, 3.21, 1.5)$. leads to chaotic dynamics, see Figure 6(a). (There is a very short transient in this data set.) Figure 6(b) shows the translation components (v_1, v_2) of the corresponding drift along the Euclidean group orbit.

Figure 7 shows how the behaviour of the v component is Brownian-like motion not only qualitatively but also quantitatively. We consider an ensemble of 50 initial conditions with all values the same except for a range of values of w separated by 0.02. Figure 7(a) shows how the motion of the v component is Gaussian in distribution after some time. More precisely, Figure 7(b) shows that the mean drift of this ensemble is apparently very small for all times while the variance is growing linearly at a rate of approximately 3.08 units squared per time unit.

The dynamics, as is typical for chaotic behaviour, is very sensitive to parameter changes. Changing ω_1 from 3.21 to 3.20 results in a chaotic transient that locks into a high period periodic orbit. The expected drift is then quasiperiodic, see Figure 8. As a consequence, we see no reason why the rate of variance growth per unit time that characterizes the Brownian motion (in the absence of 'genuine' noise) should depend continuously on parameters in the problem. (There remains the possibility of upper semicontinuity properties such as is found for Lyapunov exponents.)

Translation symmetry In the absence of rotational/reflection symmetries, the Euclidean group is reduced to just the pure translations ($\mathbb{R}^2$). In this case a Hopf/Hopf

mode-interaction of the shape variables similarly gives rise to an extension of the form

$$\begin{aligned}
\dot{w} &= \lambda_1 w + \omega_1 x - (0.1 + y^2)w^3 \\
\dot{x} &= -\omega_1 w + \lambda_1 x - w^2 x \\
\dot{y} &= \lambda_2 y + \omega_2 z - (0.1 + w^2)y^3 \\
\dot{z} &= -\omega_2 y + \lambda_2 z - y^2 z \\
\dot{v} &= f_v(w, x, y, z)
\end{aligned} \tag{3.3}$$

where f_v has components $(f_v)_i(w, x, y, z) = b_{i1} + b_{i2}w + b_{i3}w^2 + b_{i4}w^3$; simply polynomials in w. Using the parameter values λ_i and ω_i as before, and

$$(b_{11}, b_{12}, b_{13}, b_{14}) = (-0.8, 0.2, 0.3, 0.4), \quad (b_{21}, b_{22}, b_{23}, b_{24}) = (-1.3, 0.2, 0.5, -0.2),$$

we obtain similar behaviour to the hypermeander above with the difference that (a) there is a mean drift and (b) the growth in variance is anisotropic. To illustrate this, Figure 9 shows the behaviour of v components for an ensemble of 50 trajectories generated by taking a selection of regularly spaced w values. All trajectories start at $(0, 0)$ and $t = 0$ and snapshots are shown every 50 time units. Observe that the uniform average drift rate, and a slower spread within the ensemble consistent with long term linear growth scaling the variance of a Gaussian distribution of errors. This example clearly shows evidence of an anisotropic covariance matrix, namely the lines of equiprobability are ellipses rather than circles.

4 Approximation by Brownian motion in systems with translation symmetry

In Section 3, we considered local bifurcations in systems with translation and rotation symmetry. For the case of the Hopf/Hopf mode interaction we found that chaotic dynamics in the shape variables lead in numerical simulations to random walk dynamics in the drift variables, reminiscent of the Brownian motion-like hypermeander of spiral waves observed in reaction-diffusion systems.

We now review mathematical results that go some way to explaining these simulations. In four subsections, we discuss:

(a) An example of one-dimensional diffusion [9, 6] with symmetry group $\Gamma = \mathbb{R}$.

(b) Some results of Biktashev & Holden [6] for the group $\Gamma = \mathbb{R}$, seen from an ergodic-theoretical perspective.

(c) Generalizations to the case $\Gamma = \mathbb{R}^n$ for $n \geq 2$.

(d) Generalizations to the case $\Gamma = \mathbf{SE}(n)$ for $n \geq 2$.

(a) An example of deterministic diffusion in $\mathbb{R}$

Coullet & Emilsson in [9] study Ising-Bloch wall dynamics in a modified complex Ginzburg-Landau equation

$$\partial_t u = \lambda u - \beta|u|^2 u + \alpha\partial_x^2 u + \gamma\bar{u},$$

where $u = u(x) : \mathbb{R} \to \mathbb{C}$, α, β, λ are complex parameters and $\gamma \in \mathbb{R}$. They consider time-dependent *wall solutions* $u(x,t)$ with the property that $u(x,t) \to u_\pm$ as $x \to \pm\infty$ for all t. Here $u_\pm$ are homogeneous equilibria, independent of both time and space.

If the wall solution $u(x,t)$ is itself an equilibrium, then typically there will be directed linear drift either to the left or right. Instead, Coullet & Emilsson observed for certain parameter values and initial conditions that the drift appears to be a superposition of directed linear drift motion and Brownian motion. In the cases where the linear drift is zero, they computed that the mean square displacement scales as t.

Biktashev & Holden [6] pointed out that the motion of the drift could be a consequence of chaotic motion coupled with the translation symmetry present in the problem. In particular, they showed that if the dynamics on the orbit space (modulo the translation symmetry) exhibits rapid decay of correlations, then in a frame of reference translating with constant speed, the mean square displacement (defined below, see (4.2)) satisfies

$$I(t) = \sigma^2 t + O(1),$$

where $\sigma^2 \geq 0$ is the variance (also defined below, see (4.1)). The $O(1)$ notation means that that there is a constant C such that $|I(t) - \sigma^2 t| \leq C$ for all $t > 0$.

(b) $\Gamma = \mathbb{R}$: One-dimensional deterministic Brownian motion

Local bifurcation from a uniformly traveling relative equilibrium (Ising-Bloch wall solution) leads to center bundle equations on $X \times \mathbb{R}$ of the form

$$\dot{x} = f(x), \quad \dot{v} = \phi(x)$$

where $f : X \to X$ and $\phi : X \to \mathbb{R}$. We suppose that the shape equation $\dot{x} = f(x)$ admits chaotic dynamics, as in the cases of the codimension two Hopf/Hopf mode-interaction discussed in Section 3(c).

To simplify the exposition, we first consider the easier case of discrete time dynamics. That is, we consider iteration of a diffeomorphism $F : X \times \mathbb{R} \to X \times \mathbb{R}$ of the form

$$F(x,v) = (f(x), v + \phi(x))$$

where $f : X \to X$ and $\phi : X \to \mathbb{R}$. Iterating,

$$F^N(x, v) = (f^N(x), v_N(x)), \quad \text{where} \quad v_N = v + \textstyle\sum_{j=0}^{N-1} \phi \circ f^j.$$

The mapping ϕ can be viewed as a smooth observation on the (nonequivariant) dynamical system X. Results of a statistical nature about the partial sums $\sum_{j=0}^{N-1} \phi \circ f^j$ correspond directly to results about the translation drift.

Mean drift If μ is an ergodic measure on X (supported on Λ say), then the ergodic theorem states that

$$\tfrac{1}{N} v_N(x) \to \textstyle\int_X \phi \, d\mu \quad \text{as } N \to \infty,$$

for μ-almost every $x \in X$. In other words, the translation drift at time N satisfies

$$v_N = N\bar{v} + o(N) \quad \text{as } N \to \infty,$$

for almost every initial condition, where $\bar{v} = \int_X \phi \, d\mu$ is the mean drift. Provided $\bar{v} \neq 0$ (which is typical since there are no restrictions on ϕ), we have linear drift.

Now suppose that $\Lambda \subset X$ is a topologically mixing hyperbolic basic set equipped with a Gibbs measure μ. In particular, μ is an ergodic measure. Typically, there is linear drift, but by passing to a moving frame, we can set $\bar{v} = 0$. In other words, we restrict attention to observations with mean zero ($\int \phi = 0$). The statistical properties of hyperbolic basic sets are well-understood; see the books by Ruelle [36], Bowen [8] and Parry & Pollicott [31].

Decay of correlations Suppose that $\Lambda \subset X$ is a topologically mixing hyperbolic basic set. For each smooth observation $\phi : X \to \mathbb{R}$ with mean zero, there are constants $\rho \in (0, 1)$ and $C > 0$ such that $|\int \phi(\phi \circ f^j)| \leq C\rho^j$ for all $j \geq 1$. This property is known as *exponential decay of correlations*.

Variance Suppose that $\bar{v} = \int \phi = 0$. It follows easily from decay of correlations that $\frac{1}{N} \int v_N^2$ converges as $N \to \infty$. Define the *variance* $\sigma^2 = \lim_{N\to\infty} \frac{1}{N} \int v_N^2$. Then $\sigma^2 \in [0, \infty)$. Moreover,

$$\textstyle\int v_N^2 = N\sigma^2 + O(1) \quad \text{as } N \to \infty. \tag{4.1}$$

The degenerate case $\sigma = 0$ occurs if and only if v_N is uniformly bounded on Λ. In fact, $\sigma > 0$ for an open and dense set of smooth functions $\phi : X \to \mathbb{R}$.

Mean square displacement Next, define the *mean square displacement*

$$I(N) = \lim_{J\to\infty} \frac{1}{J} \sum_{j=0}^{J-1} (\phi \circ f^{j+N} - \phi \circ f^j)^2 \tag{4.2}$$

as a map from X to $\mathbb{R}^+$. It follows from the ergodic theorem that this limit exists almost everywhere and indeed that $I(N) = \int v_N^2$ almost everywhere. Hence,

$$I(N) = N\sigma^2 + O(1) \quad \text{as } N \to \infty,$$

almost everywhere. This recovers the results of Biktashev & Holden [6].

Central limit theorem A deterministic central limit theorem (CLT) for topologically mixing hyperbolic basic sets (Ruelle [36, p. 102]) states that $\frac{1}{\sqrt{N}} v_N$ converges in distribution to a normal distribution $N(0, \sigma^2)$ with mean zero and variance σ^2.

Weak invariance principle There is a refinement of the CLT known as the weak invariance principle (WIP) (or functional CLT). This result follows from the results of Denker and Philipp [10] described below and also from [16].

We define a sequence of *random elements* $W_N : X \to C([0,\infty), \mathbb{R})$ (where the variable $t \in [0,\infty)$ represents time) taking the value 0 at $t = 0$ and

$$W_N(t) = \tfrac{1}{\sqrt{N}} v_{Nt}, \quad \text{for } t = 1/N, 2/N, \cdots \tag{4.3}$$

Let W denote Brownian motion with variance σ^2 (so for each t, the random variable $W(t)$ has variance $t\sigma^2$). Then the sequence of random elements W_N converges in distribution to W inside $C([0,\infty), \mathbb{R})$. See [7] for precise definitions.

A consequence of the WIP is that for each continuous function $\chi : C([0,\infty), \mathbb{R}) \to \mathbb{R}$, the corresponding sequence of random variables $\chi(W_N)$ converges in distribution to the random variable $\chi(W)$. Taking χ to be evaluation at $t = 1$, we recover the CLT.

Almost sure invariance principle Denker and Philipp [10] prove an 'almost sure invariance principle' (ASIP) whereby there is a random element S taking values in $C([0,\infty), \mathbb{R})$ such that the sequences $\{v_N;\ N \geq 1\}$ and $\{S(N);\ N \geq 1\}$ are equal in distribution and for $\delta > 0$ sufficiently small,

$$S(t) = W(t) + O(t^{1/2-\delta}) \quad \text{as } t \to \infty, \tag{4.4}$$

almost everywhere. Again, W is Brownian motion with variance σ^2.

To summarize, we have the following result.

Theorem 4.1 *Suppose that $\Lambda \subset X$ is a topologically mixing hyperbolic basic set and $\phi : X \to \mathbb{R}$ is smooth. Let $\bar{v} = \int \phi$ and $\sigma^2 = \lim_{N\to\infty} \frac{1}{N} \int (v_N - N\bar{v})^2$. Then for an open dense set of smooth ϕ, and for almost all initial conditions, the translation drift is a superposition of a linear directed drift with velocity $\bar{v} \neq 0$ and a motion that is asymptotically Brownian motion with variance $\sigma^2 > 0$.* ∎

Law of the iterated logarithm The ASIP (4.4) subsumes all of the previous results, as well as the functional law of the iterated logarithm [32]. The latter result implies the standard law of the iterated logarithm (LIL): if $\bar{v} = \int \phi = 0$, then

$$\limsup_{N\to\infty} v_N / \sqrt{2N \log\log N} = \sigma \quad \text{almost everywhere.}$$

Flows The case of a skew-product flow on $X \times \mathbb{R}$ is similar to the case of a diffeomorphism, but with some technical complications. The skew product equations take the form

$$\dot{x} = f(x), \quad \dot{v} = \phi(x),$$

where $f : X \to X$, $\phi : X \to \mathbb{R}$. Suppose that $x(t)$ is the solution to the $\dot{x}$ equation (with initial condition $x(0) = x_0$ say), then the solution to the $\dot{v}$ equation with initial condition $v(0) = 0$ is given by $v(t) = \int_0^t \phi(x(s))ds$. If μ is an ergodic measure on X and $\bar{v} = \int_X \phi \, d\mu$, then

$$v(t) = t\bar{v} + o(t), \quad \text{as } t \to \infty,$$

for almost every initial condition x_0. Again, it is typically the case that $\bar{v} \neq 0$.

Statistical results such as exponential decay of correlations are much harder for hyperbolic flows than for diffeomorphisms, see for example [37, 34]. (For substantial recent progress, see [12, 13] and references therein.) Nevertheless, under certain technical assumptions on the mean zero function ϕ, Denker & Philipp [10] prove that the translation drift $v(t)$ is a superposition of a linear directed drift with velocity $\bar{v} \neq 0$ and a motion that is asymptotically Brownian motion with variance $\sigma^2 > 0$. This is an analogue of Theorem 4.1 for flows.

(c) $\Gamma = \mathbb{R}^n$: nonstandard n-dimensional deterministic Brownian motion

Consider a skew product diffeomorphism $F : X \times \mathbb{R}^n \to X \times \mathbb{R}^n$. So $F(x, v) = (f(x), +\phi(x))$ where $f : X \to X$ and $\phi : X \to \mathbb{R}^n$. Iterating,

$$F^N(x, v) = (f^N(x), v_N(x)), \quad \text{where} \quad v_N = v + \textstyle\sum_{j=0}^{N-1} \phi \circ f^j.$$

Again, we suppose that Λ is a topologically mixing hyperbolic basic set equipped with a Gibbs measure μ. Define the mean drift $\bar{v} = \int \phi$. As before, we have that

$$v_N = N\bar{v} + o(N) \quad \text{as } N \to \infty,$$

for almost every initial condition.

Passing to a moving frame so that $\bar{v} = \int \phi = 0$, we obtain n-dimensional analogues of the results for $X \times \mathbb{R}$. The variance σ^2 is replaced by an $n \times n$-dimensional covariance matrix Σ satisfying

$$\int v_N v_N^T = N\Sigma + O(1).$$

Note that Σ is symmetric and positive-semidefinite. Again, $\Sigma = 0$ if and only if v_N is uniformly bounded. The conditions for nondegeneracy ($\det \Sigma > 0$) are more complicated: $\det \Sigma = 0$ if and only if πv_N is uniformly bounded on Λ for some projection $\pi : \mathbb{R}^n \to \mathbb{R}$. Moreover, $\det \Sigma > 0$ for an open and dense set of smooth functions $\phi : X \to \mathbb{R}$. Indeed Σ is a *general* $n \times n$ symmetric positive-definite symmetric matrix, cf. [29].

The *mean square displacement*

$$I(N) = \lim_{J \to \infty} \frac{1}{J} \sum_{j=0}^{J-1} |\phi \circ f^{j+N} - \phi \circ f^j|^2. \tag{4.5}$$

satisfies

$$I(N) = N \operatorname{tr} \Sigma + O(1) \quad \text{as } N \to \infty,$$

almost everywhere.

An n-dimensional CLT (Ruelle [36, p. 102]) implies that $\frac{1}{\sqrt{N}} v_N$ converges in distribution to an n-dimensional normal distribution $N(0, \Sigma)$ with mean zero and covariance matrix Σ. Similarly, we obtain an n-dimensional version [16] of the WIP. Define a sequence of random elements $W_N \in C([0, \infty), \mathbb{R}^n)$ using formula (4.3) and let W denote n-dimensional Brownian motion with covariance matrix Σ. Then W_N converges in distribution to W inside of $C([0, \infty), \mathbb{R}^n)$.

The following version of the LIL is proved in [16]. For each $c \in \mathbb{R}^n$,

$$\limsup_{N \to \infty} \; c \cdot v_N / \sqrt{2N \log \log N} = \sigma_c \quad \text{almost everywhere,}$$

where $\sigma_c^2 = c \cdot \Sigma c$.

Finally, we turn to the ASIP. The following result is conjectured in [16].

Conjecture 4.2 *Suppose that $\Lambda \subset X$ is a topologically mixing hyperbolic basic set and that $\phi : X \to \mathbb{R}^n$ is smooth. Suppose further that $\bar{v} = \int \phi = 0$ and $\det \Sigma > 0$.*

Then there is a random element S taking values in $C([0,\infty), \mathbb{R}^n)$ such that the sequences $\{v_N;\ N \geq 1\}$ and $\{S(N);\ N \geq 1\}$ are equal in distribution and for $\delta > 0$ sufficiently small,

$$S(t) = W(t) + O(t^{1/2-\delta}) \quad \text{as } t \to \infty,$$

almost everywhere. Again, W is Brownian motion with covariance Σ. ∎

The following weaker result is proved in [16].

Theorem 4.3 *Assume the hypotheses of Conjecture 4.2.*

For each vector $c \in \mathbb{R}^n$, there is a random element S_c taking values in $C([0,\infty), \mathbb{R})$ such that the sequences $\{c \cdot v_N;\ N \geq 1\}$ and $\{S_c(N);\ N \geq 1\}$ are equal in distribution and for $\delta > 0$ sufficiently small,

$$S_c(t) = c \cdot W(t) + O(t^{1/2-\delta}) \quad \text{as } t \to \infty,$$

almost everywhere. ∎

(d) $\Gamma = \mathbf{SE}(n)$: standard n-dimensional deterministic Brownian motion

When $\Gamma = \mathbf{SE}(n) = \mathbf{SO}(n) \ltimes \mathbb{R}^n$, the skew product diffeomorphism $F : X \times \mathbf{SE}(n) \to X \times \mathbf{SE}(n)$ takes the form

$$F(x, g, v) = (f(x), gh(x), v + gk(x)),$$

where $f : X \to X$, $h : X \to \mathbf{SO}(n)$ and $\phi : X \to \mathbb{R}^n$. It is convenient to write

$$F(x, g, v) = (S(x, g), v + \phi(x, g)),$$

where $S(x, g) = (f(x), gh(x))$ is a skew product diffeomorphism on $X \times \mathbf{SO}(n)$. In this way, we can view F as an $\mathbb{R}^n$ extension of the diffeomorphism S. Iterating,

$$F^N(x, v) = (S^N(x, g), v_N(x, g)), \quad \text{where} \quad v_N = v + \textstyle\sum_{j=0}^{N-1} \phi \circ S^j.$$

Once again, we suppose that $\Lambda \subset X$ is a topologically mixing hyperbolic basic set equipped with a Gibbs measure μ. The corresponding invariant set $\Lambda \times \mathbf{SO}(n) \subset X \times \mathbf{SO}(n)$ is an example of a *partially hyperbolic* basic set. It is important to keep in mind that $\phi : X \times \mathbf{SO}(n) \to \mathbb{R}^n$ has the special structure $\phi(x, g) = gk(x)$. This is equivalent to saying that $\phi : X \times \mathbf{SO}(n) \to \mathbb{R}^n$ is $\mathbf{SO}(n)$-equivariant in the sense that $\phi(x, ag) = a \cdot \phi(x, g)$ for all $a \in \mathbf{SO}(n)$. To summarize, we have shown that the translation drift on $X \times \mathbf{SE}(n)$ can be studied in terms of the statistics of $\mathbf{SO}(n)$-equivariant observations on the partially hyperbolic set $X \times \mathbf{SO}(n)$.

Proposition 4.4 *If $\phi : X \times \mathbf{SO}(n) \to \mathbb{R}^n$ is an equivariant observation, and $n \geq 2$, then ϕ has mean zero. That is, the mean drift $\bar{v}$ is automatically zero.*

Proof Let $P = \int_{\mathbf{SO}(n)} g \, d\nu : \mathbb{R}^n \to \mathbb{R}^n$. We claim that $P = 0$. Let $a \in \mathbf{SO}(n)$. Then $\int_{\mathbf{SO}(n)} ag \, d\nu = \int_{\mathbf{SO}(n)} g \, d\nu$ by the translation invariance of Haar measure. Hence $aP = P$ so that $aPv = Pv$ for all $a \in \mathbf{SO}(n)$ and all $v \in \mathbb{R}^n$. (In other words, P is projection onto the fixed-point space of the action of $\mathbf{SO}(n)$ on $\mathbb{R}^n$.) But $\mathbf{SO}(n)$ acts fixed-point freely on $\mathbb{R}^n$ (since $n \geq 2$) and so $Pv = 0$ for all v proving the claim.

Writing $\phi(x, g) = gk(x)$, we compute that

$$\int_{X \times \mathbf{SO}(n)} \phi(x, g) dm = (\int_{\mathbf{SO}(n)} g \, d\nu)(\int_X k d\mu) = P \int_X k d\mu = 0$$

as required. ∎

Of course, if $X \times \mathbf{SO}(n)$ is the trivial extension of X ($h \equiv e$), then $X \times \mathbf{SO}(n)$ is not ergodic and no interesting results are possible. It turns out [17, 30] that $\mathbf{SO}(n)$ extensions are typically ergodic, and even weak mixing. From now on, we assume that $\Lambda \times \mathbf{SO}(n)$ is weak mixing with respect to the measure $m = \mu \times \nu$. It follows from ergodicity and Proposition 4.4 that $v_N = o(N)$ grows sublinearly for almost every initial condition in $X \times \mathbf{SO}(n)$, and there is no directed linear drift.

Although Dolgopyat [11] has counter-examples to decay of correlations for general observations on $\Lambda \times \mathbf{SO}(n)$, it turns out that exponential decay of correlations holds for smooth $\mathbf{SO}(n)$-equivariant observations [16]. Hence, we can define the covariance matrix $\Sigma = \lim_{N \to \infty} \frac{1}{N} \int v_N v_N^T$. It is easy to see that Σ is an $\mathbf{SO}(n)$-equivariant matrix: $\Sigma g = g\Sigma$ for all $g \in \mathbf{SO}(n)$. It follows from irreducibility of the action of $\mathbf{SO}(n)$ on $\mathbb{R}^n$ that $\Sigma = \sigma^2 I_n$ where $\sigma^2 \geq 0$. Again, $\sigma = 0$ if and only if v_N is uniformly bounded, and typically $\sigma > 0$, see Nicol *et al.* [29].

The mean square displacement as defined in (4.5) satisfies

$$I(N) = Nn\sigma^2 + O(1) \quad \text{as } N \to \infty$$

almost everywhere. In addition, the CLT, WIP, LIL and ASIP for $\mathbb{R}^n$-extensions (Subsection (c)), carry over to the case of $\mathbf{SE}(n)$-extensions with the obvious modifications; namely that we restrict to $\mathbf{SO}(n)$-equivariant functions $\phi : X \times \mathbf{SO}(n) \to \mathbb{R}^n$ which automatically have zero mean and covariance matrix of the form $\Sigma = \sigma^2 I_n$.

For example, the LIL states that for each unit vector $c \in \mathbb{R}^n$,

$$\limsup_{N \to \infty} \; c \cdot v_N / \sqrt{2N \log \log N} = \sigma \quad \text{almost everywhere.}$$

5 Discussion

In this paper, we have presented a scenario giving onset of hypermeander of spiral waves in excitable media in terms of a codimension two bifurcation in a dynamical system with Euclidean symmetry. We have also indicated how Brownian-like behaviour superimposed on a linear drift arises for PDEs that have translation symmetry but no rotation symmetry. Our explanation combines techniques from both local bifurcation theory and from global dynamics/ergodic theory.

However, one needs to be aware that there are some gaps in a completely rigorous understanding and therefore one has to make several caveats:

1. There is no proof that the supposed steady-state/Hopf or Hopf/Hopf bifurcation takes place in the FitzHugh-Nagumo model or indeed any PDE model of an excitable system such as the BZ reaction. It is accepted that meandering spirals do occur through Hopf bifurcation [5, 41], and so more complicated behavior documented in Winfree [42] is strongly indicative of a higher codimension bifurcation nearby, but it may not necessarily be associated with a local bifurcation. Other bifurcations that would be expected to lead to hypermeander by the same arguments are period doubling cascades, crises and homoclinic bifurcations.

2. The results of [29, 16] assume one has a discrete time system with hyperbolic base dynamics. In the steady-state/Hopf and Hopf/Hopf mode-interactions, time is continuous and although there exist hyperbolic saddles (in the form of horseshoes), the chaotic attractors are at best nonuniformly hyperbolic. The extension to continuous time looks feasible in the case of shift dynamics (following [13]) and would imply the existence of (unstable) solutions exhibiting hypermeander, corresponding to horseshoes in the base dynamics. This is the subject of work in progress. The extension to continuous time and nonuniformly hyperbolic base dynamics is a much more difficult problem.

3. On a more technical level, the center bundle reduction of [39] requires a spectral hypothesis that is surely invalid as it stands [40]. Nevertheless, the successful explanation of meandering and linear drift [14, 18] is strongly suggestive that many aspects of the theory do not require the full strength of this hypothesis. (One place where the non-validity of this hypothesis definitely leads to problems is documented in [2, p. 752] but this appears to be an exceptional situation.)

In the past, the very existence of hypermeander in PDE models has been somewhat controversial since longer numerical simulations often reduce hypermeander to a long complicated transient [6, footnote 4]. This effect can be explained in the context of our model since the chaotic dynamics in mode-interactions often occurs in exponentially

thin wedges in parameter space and hence near onset, hypermeander is difficult to find and the spiral structure may be lost through other instabilities well before the chaos from the mode-interaction becomes noticeable. The ODE model makes it easy to find parameters yielding the desired chaos and hence hypermeander. This should be contrasted with simulation of a poorly understood phenomenon in the PDE models.

Acknowledgments We are grateful to Bernold Fiedler and John Guckenheimer for helpful suggestions. The research of IM was supported in part by NSF Grant DMS-0071735. The research of MN was supported in part by EPSRC Grant GR/L98923.

References

[1] P. Ashwin and I. Melbourne. Noncompact drift for relative equilibria and relative periodic orbits. *Nonlinearity* **10** (1997) 595–616.

[2] P. Ashwin, I. Melbourne and M. Nicol. Drift bifurcations of relative equilibria and transitions of spiral waves. *Nonlinearity* **12** (1999) 741-755.

[3] P. Ashwin, I. Melbourne and M. Nicol. Drift for Euclidean extensions of dynamical systems. *Equadiff 99, International Conference on Differential Equations*, (B. Fiedler *et al.* eds.) World Scientific, Singapore, 2000, 145–150.

[4] D. Barkley. Euclidean symmetry and the dynamics of rotating spiral waves. *Phys. Rev. Lett.* **72** (1994) 164–167.

[5] D. Barkley, M. Kness and S. Tuckerman. Spiral-wave dynamics in a simple model of excitable media: The transition from simple to compound rotation. *Phys. Rev. A* **42** (1990) 2489–2492.

[6] V. N. Biktashev and A. Holden. Deterministic Brownian motion in the hypermeander of spiral waves. *Physica D* **116** (1998) 342–354.

[7] P. Billingsley. Convergence of Probability Measures. Wiley, New York, 1968.

[8] R. Bowen. *Equilibrium States and the Ergodic Theory of Anosov Diffeomorphisms*. Lecture Notes in Math. **470**, Springer, Berlin, 1975.

[9] P. Coullet and K. Emilsson. Chaotically induced defect diffusion. *Instabilities and Nonequilibrium Structures, V*. Kluwer, 1996, pp. 55–62.

[10] M. Denker and W. Philipp. Approximation by Brownian motion for Gibbs measures and flows under a function. *Ergod. Th. & Dynam. Sys.* **4** (1984) 541–552.

[11] D. Dolgopyat. On mixing properties of compact group extensions of hyperbolic systems. Preprint.

[12] D. Dolgopyat. Prevalence of rapid mixing in hyperbolic flows. *Ergod. Th. & Dynam. Sys.* **18** (1998) 1097–1114.

[13] D. Dolgopyat. Prevalence of rapid mixing — II: topological prevalence. *Ergod. Th. & Dynam. Sys.* **20** (2000) 1045–1059.

[14] B. Fiedler, B. Sandstede, A. Scheel and C. Wulff. Bifurcation from relative equilibria to non-compact group actions: Skew products, meanders, and drifts. *Doc. Math. J. DMV* **1** (1996) 479–505.

[15] B. Fiedler and D. V. Turaev. Normal forms, resonances, and meandering tip motions near relative equilibria of Euclidean group actions. *Arch. Rational Mech. Anal.* **145** (1998) 129–159.

[16] M. J. Field, I. Melbourne and A. Török. Decay of correlations, central limit theorems and approximation by Brownian motion for compact Lie group extensions. (In preparation, 2001).

[17] M. J. Field and W. Parry. Stable ergodicity of skew extensions by compact Lie groups. *Topology* **38** (1999) 167–187.

[18] M. Golubitsky, V. G. LeBlanc and I. Melbourne. Meandering of the spiral tip — an alternative approach. *J. Nonlinear Sci.* **7** (1997) 557–586.

[19] M. Golubitsky, V. G. LeBlanc and I. Melbourne. Hopf bifurcation from rotating waves and patterns in physical space. *J. Nonlinear Sci.* **10** (2000) 69–101.

[20] J. Guckenheimer and P. Holmes. *Nonlinear Oscillations, Dynamical Systems, and Bifurcations of Vector Fields.* Appl. Math. Sci. **42**, Springer, New York, Heidelberg, Berlin, 1990.

[21] J. Guckenheimer, M. R. Myers, F. J. Wicklin and P. A. Worfolk. *Dstool: a dynamical systems toolkit with an interactive graphical interface, user's manual* Center for Applied Mathematics, Cornell University, 1991.

[22] W. Jahnke, W. E. Skaggs and A. T. Winfree. Chemical vortex dynamics in the Belousov-Zhabotinskii reaction and in the two-variable Oregonator model. *J. Chem. Phys.* **93** (1989) 740–749.

[23] W. Jahnke and A. T. Winfree. A survey of spiral-wave behaviour in the Oregonator model. *Int. J. Bif. Chaos* **1** (1991) 445–466.

[24] J. S. W. Lamb, I. Melbourne and C. Wulff. In preparation.

[25] G. Li, Q. Ouyang, V. Petrov and H. L. Swinney. Transition from simple rotating chemical spirals to meandering and traveling spirals. *Phys. Rev. Lett.* **77** (1996) 2105–2108.

[26] E. Lugosi. Analysis of meandering in Zykov kinetics. *Physica D* **40** (1989) 331–337.

[27] R. S. MacKay and C. Tresser, Transition to topological chaos for circle maps. *Physica D* **19** (1986) 206–237.

[28] A. S. Mikhailov and V. S. Zykov. Kinematical theory of spiral waves in excitable media: comparison with numerical simulations. *Physica D* **52** (1991) 379–397.

[29] M. Nicol, I. Melbourne and P. Ashwin. Euclidean extensions of dynamical systems. *Nonlinearity* **14** (2001) 275–300.

[30] W. Parry and M. Pollicott. Stability of mixing for toral extensions of hyperbolic systems. *Proc. Steklov Inst.* **216** (1997) 354–363.

[31] W. Parry and M. Pollicott. *Zeta Functions and the Periodic Orbit Structure of Hyperbolic Dynamics*. Astérique **187-188**, Société Mathématique de France, Montrouge, 1990.

[32] W. Philipp and W. F. Stout. *Almost Sure Invariance Principles for Partial Sums of Weakly Dependent Random Variables*. Memoirs of the Amer. Math. Soc. **161**, Amer. Math. Soc., Providence, RI, 1975.

[33] T. Plesser, S. C. Müller and B. Hess. Spiral wave dynamics as a function of proton concentration in the ferroin-catalyzed Belousov-Zhabotinskii reaction. *J. Phys. Chem.* **94** (1990) 7501–7507.

[34] M. Pollicott. On the rate of mixing of Axiom A flows. *Invent. Math.* **81** (1985) 413–426.

[35] O. E. Rossler and C. Kahlert. Winfree meandering in a 2-dimensional 2-variable excitable medium. *Z. Naturforsch.* **34** (1979) 565–570.

[36] D. Ruelle. *Thermodynamic Formalism*. Encyclopedia of Math. and its Applications **5**, Addison Wesley, Massachusetts, 1978.

[37] D. Ruelle. Flows which do not exponentially mix. *C. R. Acad. Sci. Paris* **296** (1983) 191–194.

[38] B. Sandstede, A. Scheel and C. Wulff. Center-manifold reduction for spiral waves. *C. R. Acad. Sc., Série I, Math.* **324** (1997) 153–158.

[39] B. Sandstede, A. Scheel and C. Wulff. Dynamics of spiral waves on unbounded domains using center-manifold reductions. *J. Diff. Eq.* **141** (1997) 122–149.

[40] A. Scheel. Bifurcation to spiral waves in reaction-diffusion systems. *SIAM J. Math. Anal.* **29** (1998) 1399–1418.

[41] G. S. Skinner and H. L. Swinney. Periodic to quasiperiodic transition of chemical spiral rotation. *Physica D* **48** (1991) 1–16.

[42] A. T. Winfree. Varieties of spiral wave behaviour: an experimentalist's approach to the theory of excitable media. *Chaos* **1** (1991) 303–334.

[43] C. Wulff. Theory of meandering and drifting spiral waves in reaction-diffusion systems. Dissertation, FU Berlin, 1996.

[44] V. S. Zykov. Cycloidal circulation of spiral waves in an excitable medium. *Biofizika* **31** (1986) 862–865.

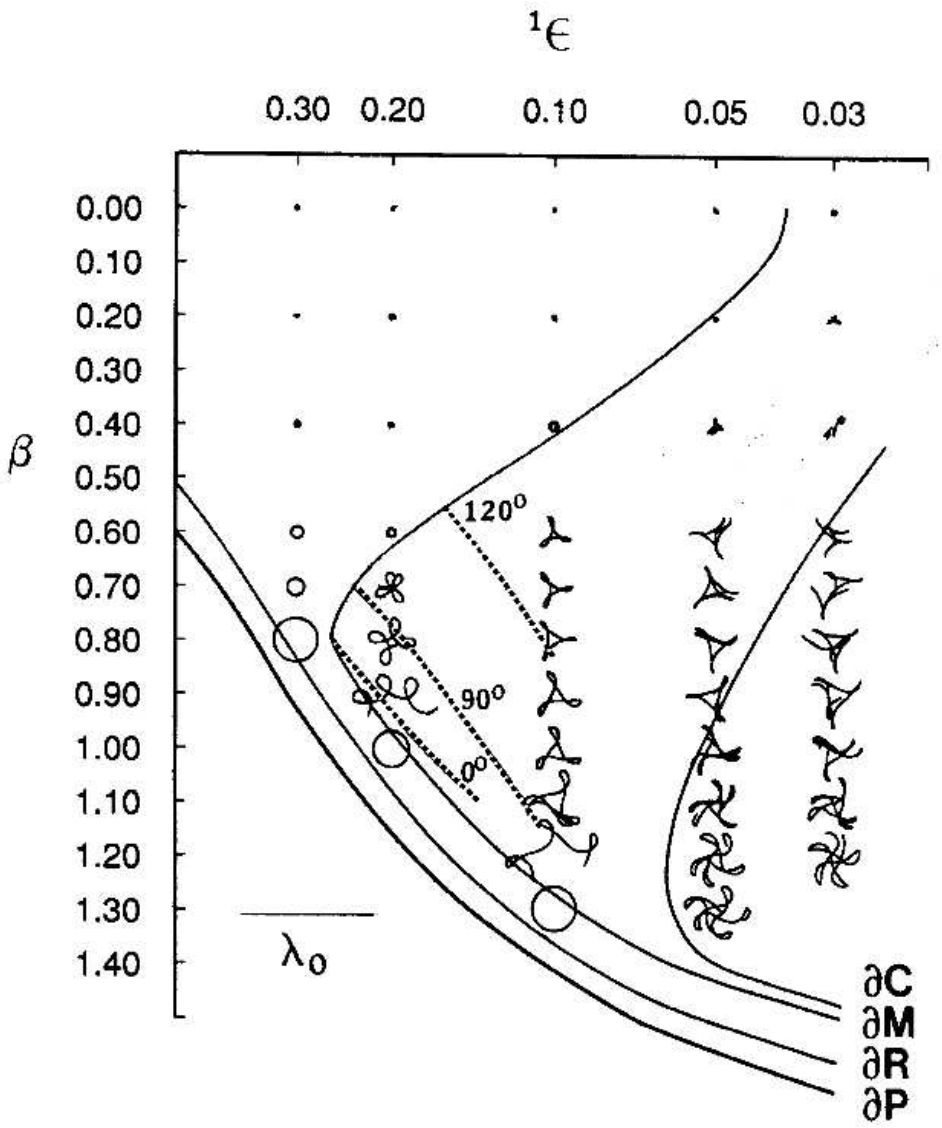

Figure 1: Spiral transitions in the FitzHugh-Nagumo (FHN) equation. ϵ and β are parameters in the FHN equation. Adapted with permission from Winfree [42]. Rigidly rotating spiral waves exist between ∂R and ∂M. ∂R denotes the transition from rigidly rotating spirals to retracting waves. ∂M denotes the transition from rigidly rotating spirals to meandering spirals. ∂C denotes the transition from meandering spirals to "complex" states (hypermeander).

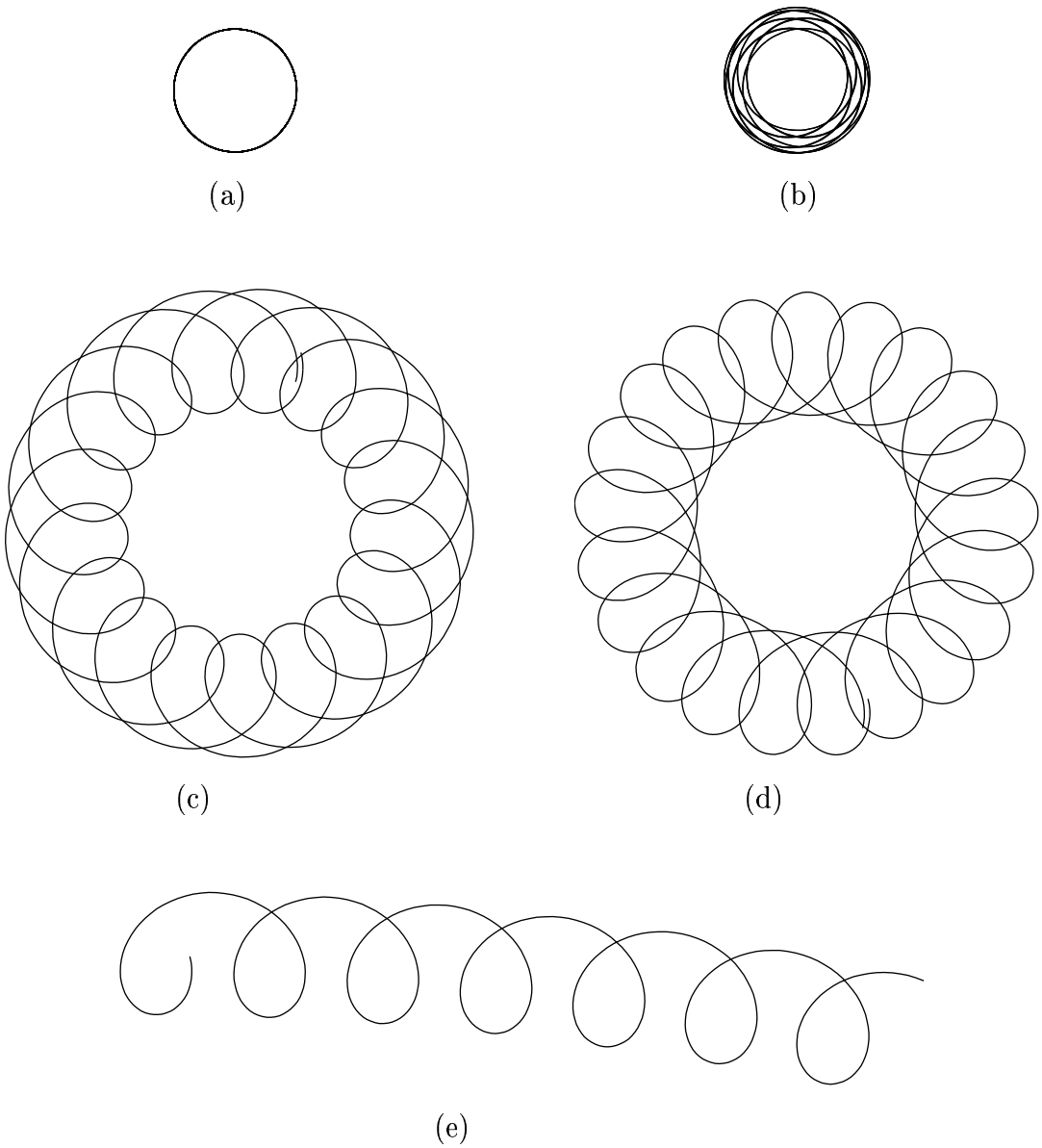

Figure 2: (a) Uniform rotation, (b) Meandering (away from resonance), (c) Meandering near resonance (petals inwards), (d) Meandering near resonance (petals outwards), (e) Linear drift. (Adapted with permission from [19].)

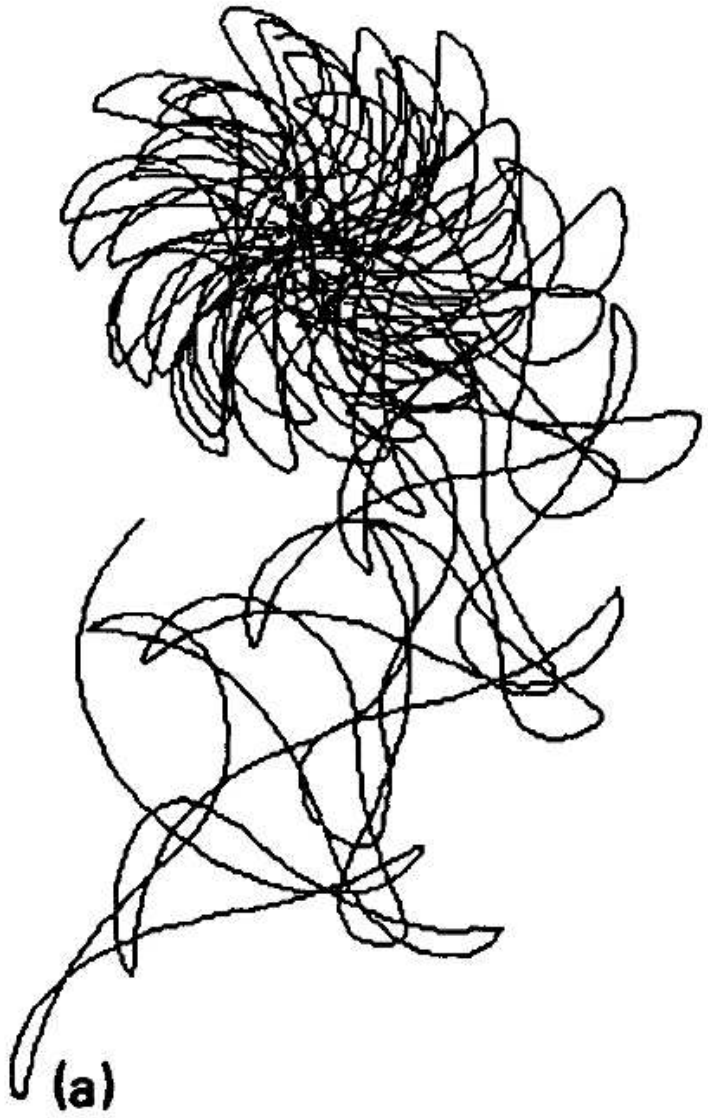

Figure 3: Transient hypermeander in the FitzHugh-Nagumo (FHN) equation. Adapted with permission from Winfree [42]

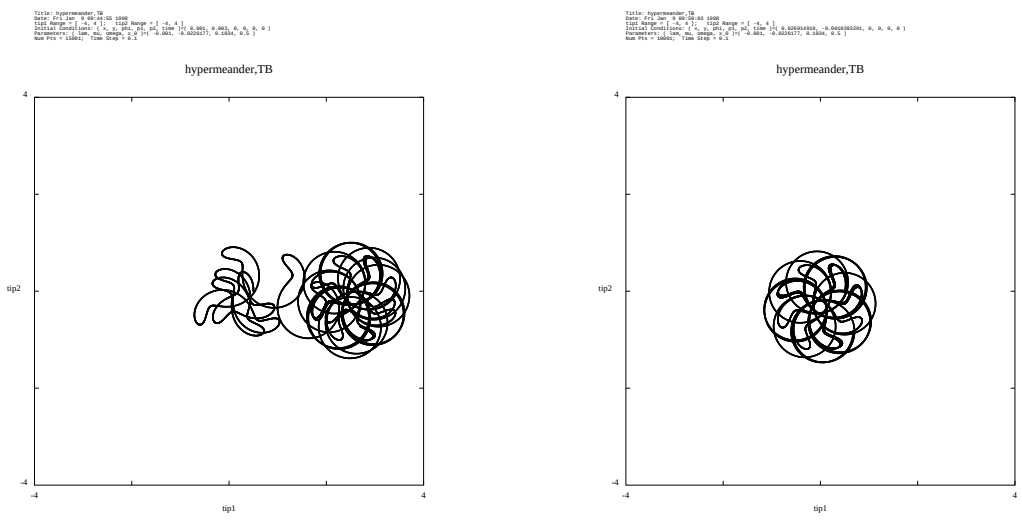

(a) (b)

Figure 4: Motion of the spiral tip in the Takens-Bogdanov bifurcation: (a) shows the chaotic transient and the eventual meandering solution. (b) shows the asymptotic dynamics without the transient

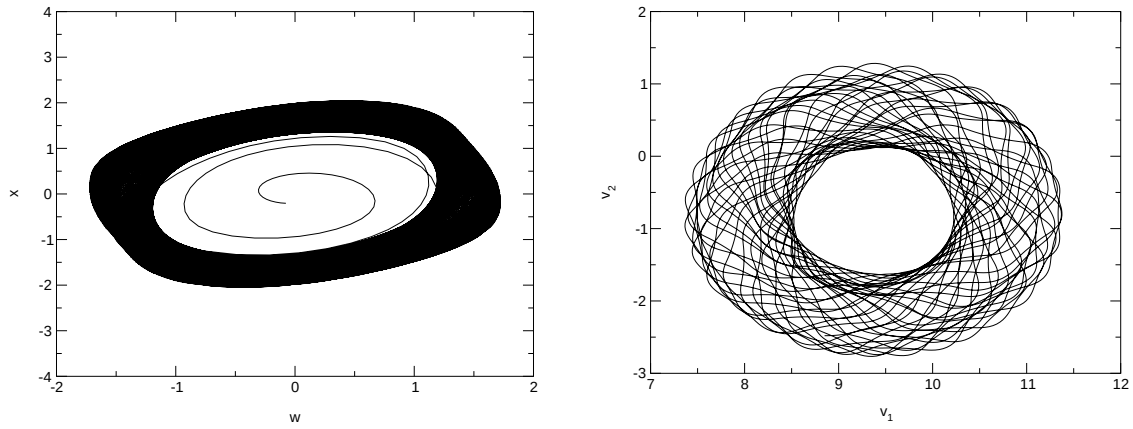

(a) (b)

Figure 5: A trajectory of system (3.2) in a regime giving quasiperiodic dynamics: (a) shows the base dynamics, projected onto the coordinates w, x, and (b) shows the evolution of the translation coordinates.

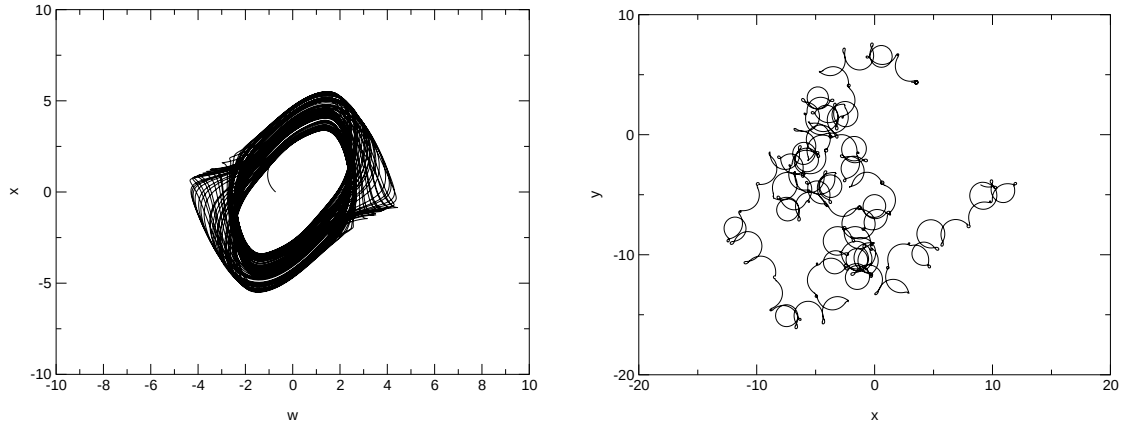

(a) (b)

Figure 6: A trajectory of system (3.2) in a regime giving hypermeander: (a) shows the base dynamics, projected onto the coordinates w, x, and (b) shows the evolution of the translation coordinates. The chaotic base dynamics induces a Brownian-type motion in the plane.

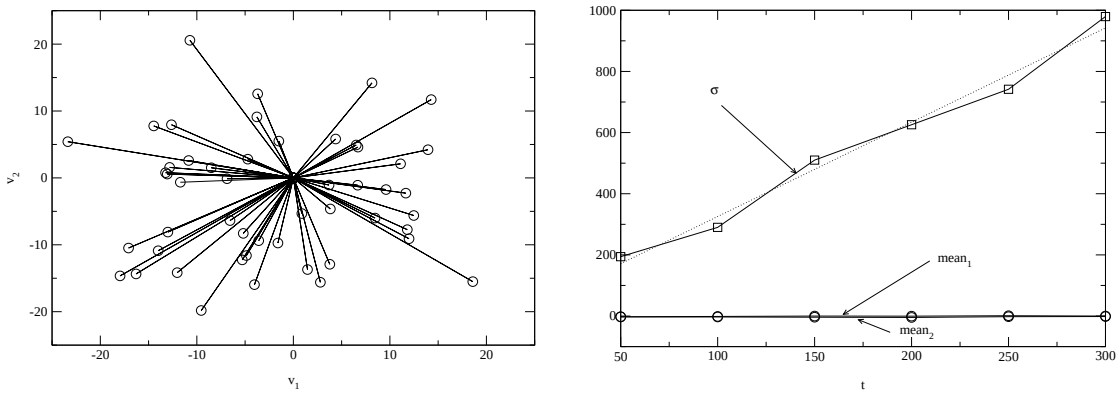

(a) (b)

Figure 7: The growth of variance for an ensemble of 50 trajectories of system (3.2) in a regime giving hypermeander. (a) illustrates the beginning and end of trajectories that start at the same point (with $v = 0$) except for w which is chosen over a range of initial values separated by 0.02. The length of integration time of all trajectories was 50. There is a clear decay of dependence on initial condition that leads to a roughly Gaussian distribution of final values of v. (b) shows the variance σ and the mean motion mean_1, mean_2 of the v-components of this ensemble of trajectories as a function of time t. As predicted, there is a Brownian-type motion where the mean drift is zero and the variance grows linearly with time.

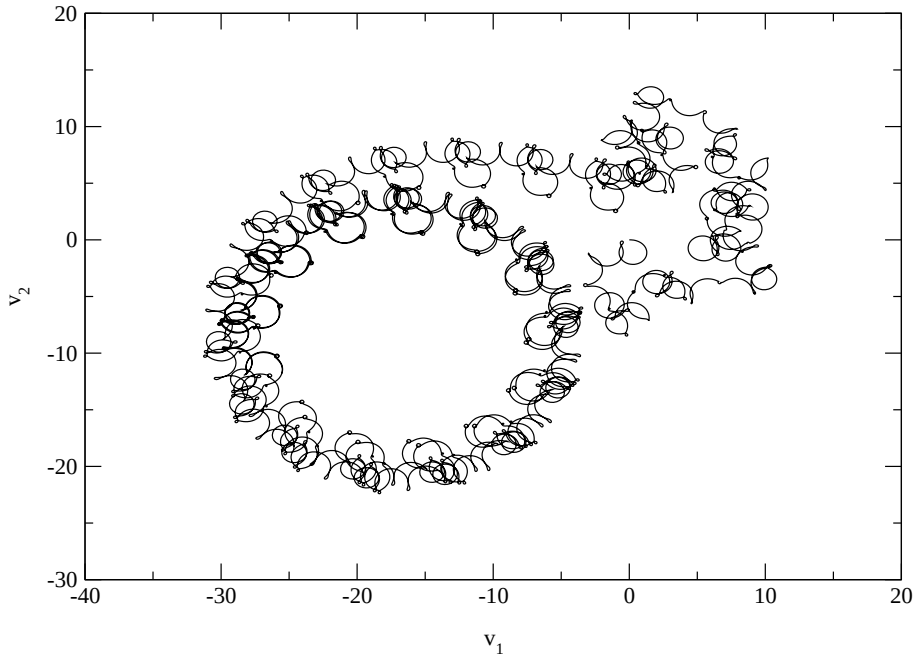

Figure 8: As in Figure 6(b) with parameters identical except that $\omega_1 = 3.20$ (instead of 3.21). The hypermeander is replaced by a chaotic transient and eventual meander.

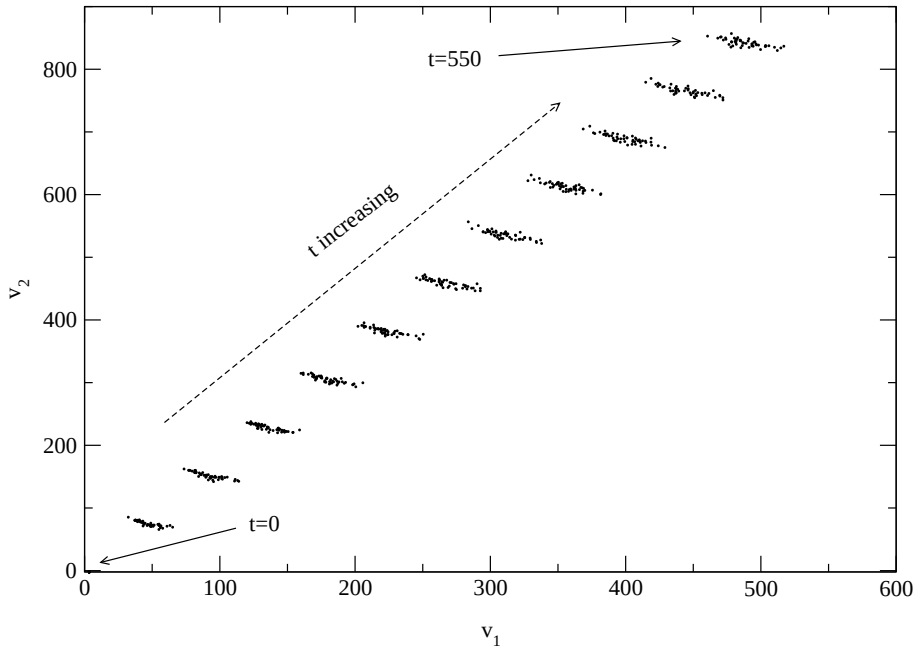

Figure 9: Determinstic diffusion in the plane. This is the pure-translation ($\mathbb{R}^2$) symmetry analogue of the hypermeander in systems with Euclidean symmetry. An ensemble of initial conditions starting at $v = 0$ evolves according to the equation (3.3). The trajectories are shown projected onto their v components at intervals of 50 time units. The linear drift is superimposed with an anisotropic Gaussian spread within the ensemble.